and variations of charged particle fluxes are associated with squeezing effects of magnetoacoustic gravity waves in general.

The most stringent test of my proposal (*11*) is whether similar discrete low-frequency modes can be directly detected in intensity variations and Doppler shifts of appropriate spectral lines (formed in the STR and the lower corona) in ultraviolet, extreme ultraviolet, and x-ray bands during the Solar and Heliospheric Observatory mission successfully launched in December 1995. A thorough understanding of these modes may offer valuable clues for the solution of longstanding problems concerning the heating and dynamics of the solar corona.

REFERENCES AND NOTES

1. D. J. Thomson, C. G. Maclennan, L. J. Lanzerotti, *Nature* **376**, 139 (1995).
2. Alfvén waves propagate along magnetic field lines; they are incompressible with magnetic field and velocity fluctuations transverse to the direction of propagation. In contrast, compressible magnetohydrodynamic perturbations include magnetic waves and magnetoacoustic gravity waves. In an appropriate low-frequency range, the latter manifest as magnetogravity waves.
3. V. C. A. Ferraro and C. Plumpton, *Astrophys. J.* **127**, 459 (1958).
4. Y.-Q. Lou and R. Rosner, *ibid.* **424**, 429 (1994).
5. Y.-Q. Lou, *J. Geophys. Res.* **98**, 3563 (1993).
6. ———, *ibid.*, p. 11483.
7. H. Hill, C. Fröhlich, M. Gabriel, V. A. Kotov, in *Solar Interior and Atmosphere*, A. N. Cox, W. C. Livingston, M. S. Matthews, Eds. (Univ. of Arizona Press, Tucson, AZ, 1991), pp. 562–617.
8. A more accurate analysis (*10*) indicates the existence of two characteristic angular frequencies closely related to ω_c and N_{BV}, respectively, with dependences on spherical harmonic degree ℓ.
9. The STR is located a few thousand kilometers above the photosphere. The atmospheric layer sandwiched between the photosphere and the transition region is referred to as the chromosphere. The STR earns its name mainly from the fact that the temperature rises drastically by two orders of magnitude across its layer thickness of a few hundred kilometers upward. The solar corona above the STR consists of a fully ionized tenuous plasma with a temperature of more than 10^6 K.
10. Y.-Q. Lou, *Mon. Not. R. Astron. Soc.* **276**, 769 (1995).
11. ———, *Astrophys. J.* **442**, 401 (1995).
12. R. G. Athay, *The Solar Chromosphere and Corona: Quiet Sun* (Reidel, Dordrecht, Netherlands, 1976); J. T. Mariska, *Annu. Rev. Astron. Astrophys.* **24**, 23 (1986).
13. N. J. Balmforth and D. O. Gough, *Astrophys. J.* **362**, 256 (1990); Y.-Q. Lou, *Astrophys. J.* **414**, L141 (1993).
14. A. Balogh *et al.*, *Science* **268**, 1007 (1995); E. J. Smith *et al.*, *Space Sci. Rev.* **72**, 165 (1995).
15. C.-H. An, S. T. Suess, R. L. Moore, Z. E. Musielak, *Astrophys. J.* **350**, 309 (1990); M. Velli, *Astron. Astrophys.* **270**, 304 (1993).
16. Y.-Q. Lou, *Mon. Not. R. Astron. Soc.* **274**, L1 (1995).
17. R. B. Leighton, R. W. Noyes, G. W. Simon, *Astrophys. J.* **135**, 474 (1962); R. B. Leighton, *Annu. Rev. Astron. Astrophys.* **1**, 19 (1963).
18. Spicules are bush-like features across the STR surrounding each individual supergranule; they appear to consist of chromospheric materials with a lifetime of about 5 to 10 min.

19. Supported by the Solar-Terrestrial Program of NSF under grants ASTR/ATM-9196237 and ATM-9320357 at the University of Chicago.

1 November 1995; accepted 27 February 1996

Probing Electrical Transport in Nanomaterials: Conductivity of Individual Carbon Nanotubes

Hongjie Dai,* Eric W. Wong,* Charles M. Lieber†

A general approach has been developed to determine the conductivity of individual nanostructures while simultaneously recording their structure. Conventional lithography has been used to contact electrically single ends of nanomaterials, and a force microscope equipped with a conducting probe tip has been used to map simultaneously the structure and resistance of the portion of the material protruding from the macroscopic contact. Studies of individual carbon nanotubes demonstrate that the structurally most perfect nanotubes have resistivities an order of magnitude lower than those found previously and that defects in the nanotube structure cause substantial increases in the resistivity.

Nanometer-scale structures and molecular materials are of great interest as potential building blocks for future generation electronic devices of greatly reduced size (*1–3*). Rational design of any device will require a fundamental understanding of the properties of these materials and how they depend on, for example, dimensionality and size. For instance, the electrical and mechanical properties of carbon nanotubes have generated considerable interest and speculation (*3–6*), although direct measurements of the intrinsic resistivity and mechanical strength of individual nanotubes has been difficult. Likewise, the term molecular wire has been widely applied to anisotropic molecular materials (*1, 2, 7*), but the meaning of this term relative to an absolute conductivity remains unclear.

The difficulty is in connecting measuring devices from the macroworld to nanometer-scale materials, for which two or more connections are needed. We report a general approach for electrical measurements of nanomaterials and have used this approach to determine the resistivity of individual carbon nanotubes. Our method combines conventional lithography, to electrically contact single ends of nanotubes, and a force microscope equipped with a conducting probe tip, to map simultaneously the structure and resistance of the portions of nanotube that protrude from the macroscopic contact. Defects in the nanotube structure cause substantial increases in the resistivity, and the structurally most perfect nanotubes have resistivities an order of magnitude lower than those found previously (*8–10*).

To measure the electrical properties of individual carbon nanotubes (Fig. 1), we deposited a drop of a nanotube suspension on a flat insulating surface and covered it with a uniform layer of Au. A pattern of open slots was produced in the Au layer by conventional lithography procedures to expose the nanotubes for measurement. Force microscopy studies showed that after this procedure, many of the single nanotubes have one end covered by the Au pattern and the other end extending into an open slot. With a conducting cantilever-tip assembly in the force microscope, it is possible to contact electrically and measure the axial conduction through a single nanotube to the Au contact while simultaneously recording the nanotube structure. Conducting tips were made by depositing NbN onto commercial Si_3N_4 cantilevers. This coating was chosen because it exhibits a combination of good conductivity and hardness. Soft conducting coatings like Au were insufficiently stable to provide reproducible measurements, and heavily doped Si tips, although robust, had excessively large contact resistances to the nanotube samples.

Our approach has some similarities to previous studies of carbon nanotubes (*9, 10*). Langer *et al.* (*9*) used a scanning tunneling microscope to identify nanotube bundles and then expose a resist so that fixed Au contacts could be made to the two ends of a bundle. Studies of nanotube bundles are limited, however, because the sizes and structures of the individual nanotubes in the ensemble are unknown. Measurement of the resistance of a single nanotube has also been reported for the chance occurrence of one nanotube spanning two lithographically patterned macroscopic electrodes (*10*). Both of these reports are two-probe experiments that can be influenced adversely by contact resistance and, in one case (*9*), the uncertainty in the structures of the nanotubes that compose the sample measured. In our studies, we can rapidly identify and focus on individual carbon nanotubes by exploiting the high-resolution imaging capabilities of the force microscope; furthermore, because we determine the resis-

H. Dai and C. M. Lieber, Department of Chemistry and Division of Applied Sciences, Harvard University, Cambridge, MA 02138, USA.
E. W. Wong, Department of Chemistry, Harvard University, Cambridge, MA 02138, USA.

*Both authors contributed equally to this work.
†To whom correspondence should be addressed.

tance at many points along the length of each tube, the contact resistance can be eliminated from our measurements.

The nanotubes used in these studies were prepared by a catalytic process (*11*, *12*). Transmission electron microscopy (TEM) analysis shows that these samples consist primarily of multishell nanotubes with diameters between 7 and 20 nm (Fig. 2). The straight nanotubes produced by this method have a relatively low density of defects and contain well-ordered concentric graphitic shells (Fig. 2B) similar to those produced by the arc-growth procedure of Iijima (*4*, *13*). The catalytic growth process also yields curved nanotubes having a much greater density of structural defects; these curved nanotubes have been exploited to investigate how defects affect electrical transport. The nanotubes produced by the catalytic process consist primarily of isolated nanotubes, not bundles, and thus can be probed individually in our experiments.

Topography and resistance maps of a single, straight carbon nanotube with a hooked end are shown in Fig. 3. A cross section perpendicular to the axis of the nanotube shows that the height of the nanotube is 13.9 nm and that the apparent width is 95 nm (Fig. 3B). The height of the nanotube as measured in topographs is consistent with TEM measurements of our nanotube samples, but the width appears unusually large. The large width is expected, however, because the images are acquired with tips having radii larger than those of the nanotubes; that is, the apparent width of the nanotube corresponds to a convolution of the larger tip radius with that of the nanotube. Importantly, the height remains unaffected by the finite tip size and therefore represents a good measure of the nanotube outer diameter. These effects have been discussed in detail for both nanotubes (*14*) and probe microscopy imaging in general (*15*). In addition, the apparent doubled structure at the lower left of Fig. 3A and in other images (for example, Fig. 4A) corresponds to multiple tips imaging an individual nanotube and not a single tip imaging a bundle of nanotubes. This conclusion is supported by Fig. 3E, where the doubled structure has changed to an identically shaped single-nanotube structure after modification of the tip, and Fig. 3F, where the entire image of this same nanotube and several small surface particles are doubled identically in an image recorded with a different tip.

The image of the nanotube in Fig. 3A shows a systematic increase in resistance from the upper right (near the connection to the Au electrode) to the lower left (where it ends) (Fig. 3C). The gray background corresponds to the insulating SiO_2 substrate. The resistance along the nanotube axis of Fig. 3C increases linearly with distance from the Au contact (Fig 3D). The total resistance R_T in this and other measurements can be ex-

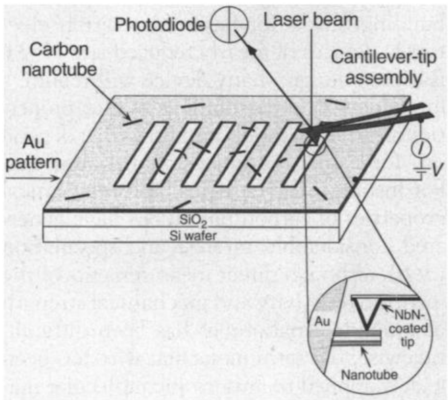

Fig. 1. Schematic diagram of the measurement of the electrical properties of an individual carbon nanotube. Nanotubes were ultrasonically dispersed in ethanol, deposited on an oxidized Si substrate, and then coated with a layer of sputtered Au. A striped pattern (4 μm by 1 mm stripes repeated every 15 μm for 2 mm) was made in the Au layer with the use of electron beam lithography to expose a resist, followed by aqueous KI/I_2 etching of the Au in the exposed regions. Control experiments demonstrated that the processing did not affect the structure of the nanotubes. Commercial Si_3N_4 cantilever-tip assemblies were coated with ~1200 Å of NbN deposited by dc magnetron sputtering. Topographic images were obtained with these cantilever tips and a commercial instrument (Nanoscope, Digital Instruments). We simultaneously made electrical measurements by recording the current flowing through the nanotube for a fixed applied voltage. The nanotube resistances determined in these measurements were independent of the sign and magnitude (between 200 and 1000 mV) of the applied voltage. Measurements were not made below 200 mV because the signal-to-noise ratio was too low.

Table 1. Summary of carbon nanotube electrical resistivities. Nanotube diameters were determined from height measurements made by taking cross sections through the topographs perpendicular to the nanotube axes. Each value represents an average obtained from several different images of the same nanotube. The linear resistance was independent of the applied voltages (200 to 1000 mV) used in these measurements. The current flowing through the nanotubes under these conditions is on the order of 1 μA; this current corresponds to a current density of ~10^6 A/cm^2. The uncertainty in resistivity ($R_s A_{cross}$) represents a combination of the uncertainties in the nanotube diameter and linear resistance determined from analysis of independent data sets acquired with different voltages on the same nanotube sample. There is also uncertainty in A_{cross}, although this is small. The values of θ, given to characterize the structure of curved nanotubes, correspond to the angle between straight lines approximating the direction of the nanotube before and after a bend in the nanotube. The three angles characterizing the structures of samples 3 and 6 indicate that there are three distinct bends along the nanotube axes of these samples.

Sample	Diameter (nm)	Linear resistance (megohms/μm)	Resistivity (ohm·m)	Structure
1	8.5	0.41	19.5 ± 2.0	Straight
2	13.9	0.06	7.8 ± 1.0	Straight
3	12.4	0.44	46.0 ± 1.8	Slowly curved over ~1 μm in length $\theta_1 \approx +5°$; $\theta_2 \approx -6°$; $\theta_3 \approx +7°$
4	15.0	0.25	37.6 ± 1.0	Slowly curved over ~1 μm in length $\theta \approx 17°$
5	18.5	0.22	48.9 ± 4.3	Moderately curved over 1 μm in length $\theta \approx 30°$
6	9.5	1.93	117 ± 19	Greatly curved over ~1 μm in length $\theta_1 \approx +80°$; $\theta_2 \approx -65°$; $\theta_3 \approx +65°$

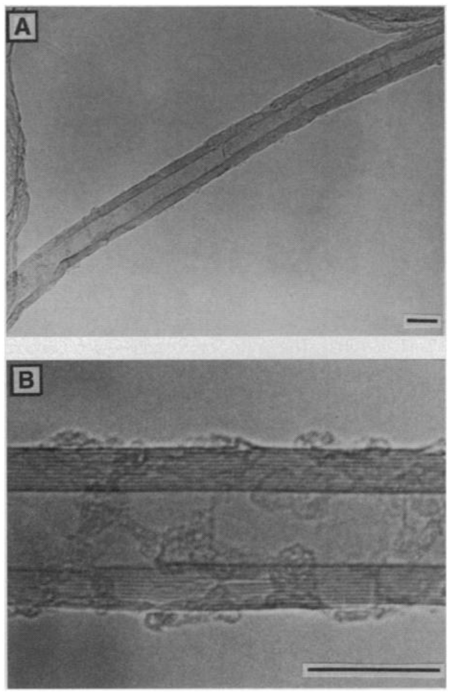

Fig. 2. (**A**) TEM image of a straight carbon nanotube produced by catalytic growth. (**B**) A high-resolution TEM image showing the multishell structure of these nanotubes. The scale bars are 10 nm. The carbon nanotubes were grown at 760°C from an ethylene-hydrogen feedstock and a supported iron catalyst (*11*, *12*).

pressed as $R_T = R_c + R_S x$, where R_c corresponds to the contact resistance in our measurement (the sum of Au-nanotube and nanotube-tip contact resistances), R_S to the linear resistance of the nanotube, and x to the position along the nanotube. Along the straight portion of this 13.9-nm-diameter nanotube, we observed a linear resistance of $R_S = 0.06$ megohms/μm. The resistance increases by more than an order of magnitude around the bend at the end of this nanotube, showing that defects can play a key role in the electrical transport of these materials. Furthermore, the resistance maps and corresponding linear slopes are stable to repetitive scanning over a several hour period, thus demonstrating that these measurements are reproducible and do not modify the sample properties.

We have obtained similar results on a number of independent nanotubes. Figure 4 shows a structural topograph and resistance map of a linear nanotube. The diameter of this nanotube determined from the topographic height is 8.5 nm; the doubling in the images is a multiple-tip effect. The resistance image (Fig. 4B) shows a systematic increase in resistance from the upper left (near to its connection to the Au contact) and the lower right (where it ends). Resistance plots taken along the nanotube axis (Fig. 4C) are similar, differing only in R_c, and are consistent with the resistance of a single nanotube determined by distinct conducting tips. The linear resistance determined for this 8.5-nm-diameter sample, 0.41 megohm/μm, is nearly 10 times that of the 13.9-nm-diameter nanotube in Fig. 3.

To compare the electrical properties of different nanotubes independently of their size, we calculated their resistivities (in microhm·meters) using the annular cross-sectional area (A_{cross}) of each sample, where $A_{cross} = \pi(r^2_{outer} - r^2_{inner})$ and r_{outer} and r_{inner} correspond to the outer and inner radii of the hollow nanotubes. The outer diameter (OD) of the nanotubes investigated in this study were determined directly from the topograph heights. Although topographs cannot provide a direct measure of the inner diameter for multishell nanotubes, extensive TEM measurements made on our samples show circular nanotubes with an annular cross-sectional area that is a well-defined function of the OD (*16*). We used this experimental relation and the ODs determined from topographs to estimate the annular areas of the individual nanotubes studied (Table 1). There are several important points to be gleaned from these data. First, straight nanotubes without obvious structural defects exhibit the lowest resistivities. Among these samples, the resistivity decreases with increasing diameter. The smallest resistivity we observed at room temperature, 7.8 microhm·m, is less than one-tenth of that obtained from macroscopic (*5, 8*) and other microscopic measurements (*9, 10*), in which the nanotube sizes and structures were uncertain. These measurements thus provide a limit to the resistivity of multishell nanotubes, although we believe our value of 7.6 microhm·m should be considered as an upper limit to the intrinsic resistivity of a perfect multishell nanotube (*17*).

Structural defects cause systematic increases in the nanotube resistivities. Comparison of samples with significant curvature [that is, samples 4 and 6 (Table 1)], which has been previously attributed to pentagonal and heptagonal defects in the nanotube structure (*3*), shows that the resistivity is almost an order of magnitude larger than that of straight nanotubes of

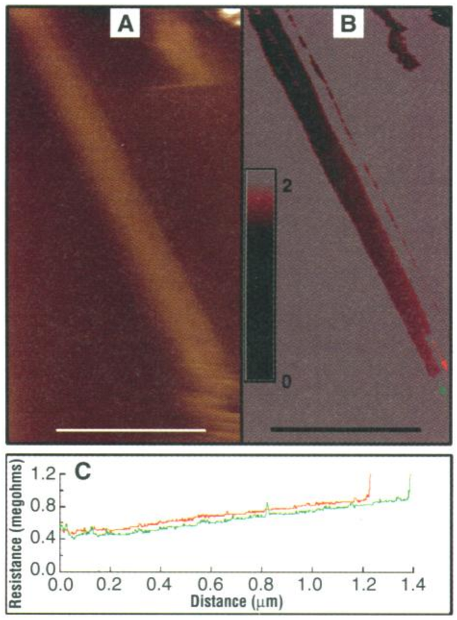

Fig. 4. (**A**) Topography and (**B**) resistance maps of a single nanotube acquired simultaneously. The nanotube-Au contact is located just outside the upper left of the images. The resistance map was acquired with an applied voltage of −240 mV and its scale is in megohms. (**C**) Two cross sections taken along the nanotube axis of the resistance map show that the resistance increases linearly away from the Au contact and increases discontinuously at the end of the tube. The scale bars in the images are 0.5 μm.

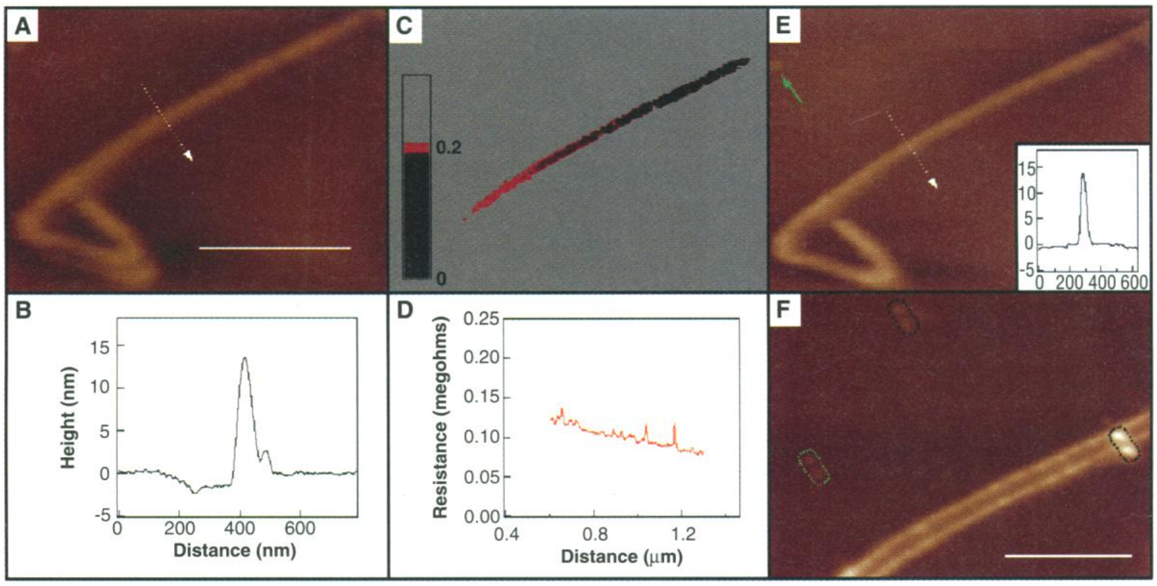

Fig. 3. (**A**) Topography, (**B**) cross section, and (**C**) resistance maps of a single nanotube acquired at the same time with the method outlined in Fig. 1. This nanotube contacts the Au overlayer beyond the upper right portion of the image. The cross section in (B) was taken along the dotted arrow in (A). The resistance map was acquired with an applied voltage of −250 mV, and its scale is in megohms. (**D**) Resistance versus length along the axis of the nanotube resistance map in (C). (**E**) Topograph of the nanotube in (A) acquired after scanning the tip for several minutes on a clean area of the SiO_2 substrate surface. The cross section (inset), taken along the dotted arrow, shows that the structure is an individual nanotube. (**F**) Topograph of the nanotube in (A) recorded with a tip before recording (A). A double tip leads to an identical doubling of all of the features in this image; doubled particles are indicated by dashed ovals. The doubled particle enclosed by the green oval corresponds to the single particle highlighted by the green arrow in (E). The scale bars in (A) and (F) are 0.5 μm.

similar diameter (that is, samples 2 and 1, respectively). We believe that this comparison demonstrates the importance of studying individual nanotubes that are structurally characterized to determine their intrinsic properties. It is also interesting to consider if it will be possible, by introducing defects directly with the probe tip or by other means, to probe systematically the effects of electron scattering in these one-dimensional structures.

The sensitivity of resistivity to structural imperfections must be accounted for to determine ultimately the intrinsic conductivity of nanotubes but may also allow tailoring of the resistance of these materials for applications. We believe that our experimental approach opens the door to developing a clear understanding of nanotube electrical transport and to testing theoretical predictions, although this will require careful studies of the temperature and diameter dependencies of the resistivity in structurally characterized samples. The approach outlined here should be applicable to probing of the intrinsic electrical properties of metal-filled nanotubes (*18*), carbide nanorods (*11*), and boron nitride nanotubes (*19*) and furthermore may be able to assess the validity of the term "molecular wire," which has been widely applied to organic and biological nanostructures (*1, 7*). Lastly, we note that the experimental approach outlined in Fig. 1 can be generalized to measure the mechanical properties of nanomaterials and thereby address their applicability in composites and other structural systems (*20*).

REFERENCES AND NOTES

1. C. A. Mirkin and M. A. Ratner, *Annu. Rev. Phys. Chem.* **43**, 719 (1992); J.-M. Lehn, *Angew. Chem. Int. Ed. Engl.* **29**, 1304 (1990); C. F. van Nostrum, S. J. Picken, A.-J. Schouten, R. J. M. Nolte, *J. Am. Chem. Soc.* **117**, 9957 (1995).
2. C.-G. Wu and T. Bein, *Science* **266**, 1013 (1994).
3. T. W. Ebbesen, *Annu. Rev. Mater. Sci.* **24**, 235 (1994).
4. S. Iijima, *Nature* **354**, 56 (1991).
5. T. W. Ebbesen and P. M. Ajayan, *ibid.* **358**, 220 (1992).
6. M. S. Dresselhaus, *ibid.*, p. 195; J. W. Mintmire, B. I. Dunlap, C. T. White, *Phys. Rev. Lett.* **68**, 631 (1992); N. Hamada, S. Sawada, A. Oshiyama, *ibid.*, p. 1579; R. Saito, M. Fujita, G. Dresselhaus, M. S. Dresselhaus, *Appl. Phys. Lett.* **60**, 2204 (1992); G. Overney, W. Zhong, D. Tomanek, *Z. Phys. D* **27**, 93 (1993).
7. C. J. Murphy *et al.*, *Science* **262**, 1025 (1993); T. J. Meade and J. F. Kayyem, *Angew. Chem. Int. Ed. Engl.* **34**, 352 (1995).
8. W. A. de Heer *et al.*, *Science* **268**, 845 (1995).
9. L. Langer *et al.*, *J. Mater. Res.* **9**, 927 (1994).
10. G. M. Whitesides and C. S. Weisbecker, *Mater. Res. Soc. Symp. Proc.* **349**, 263 (1994).
11. H. Dai, E. W. Wong, Y. Z. Lu, S. Fan, C. M. Lieber, *Nature* **375**, 769 (1995).
12. C. E. Snyder *et al.*, International Patent WO 89/07163 (1989).
13. The straight, catalytically grown nanotubes may have a higher defect density than arc-grown samples, although we believe that their overall structures are quite similar. The central objective of this work is to demonstrate an approach that can measure conductivity and structure simultaneously in nanomaterials.
14. R. Hoper *et al.*, *Surf. Sci.* **311**, L731 (1994).
15. D. L. Wilson, K. S. Kump, S. J. Eppell, R. E. Marchant, *Langmuir* **11**, 265 (1995); C. Odin, J. P. Aime, A. El Kaakour, T. Bouhacina, *Surf. Sci.* **317**, 321 (1994); J. E. Griffith and D. A. Grigg, *J. Appl. Phys.* **74**, R83 (1993).
16. The experimentally derived expression relating the annular cross-sectional area to measured OD is $A_{cross} = a + bx + cx^2$, where x is the OD in angstroms, $a = (-2.67 \pm 0.91) \times 10^{-17}$ m^2, $b = (4.73 \pm 1.6) \times 10^{-19}$ m^2/Å, and $c = (4.72 \pm 0.69) \times 10^{-21}$ m^2/Å^2.
17. Defects in multishell nanotubes increase the resistivity through electron scattering relative to an ideal structure. The lowest values we observed were still nearly a factor of 20 greater than that observed for crystalline graphite and may be an indication of scattering by such extrinsic defects. Because inner shells of multishell nanotubes cannot be probed directly by force microscopy, we believe that studies of single-shell nanotubes (*3*) ultimately provide the best measure of the intrinsic conductivity of nanotubes. It would also be possible to compare measurements of single-shell nanotubes directly with theory (*4*), whereas multishell nanotubes have not been investigated in detail theoretically.
18. P. M. Ajayan and S. Iijima, *Nature* **361**, 333 (1993); S. C. Tsang, Y. K. Chen, P. J. F. Harris, M. L. H. Green, *ibid.* **372**, 159 (1994); C. Guerret-Piecourt, Y. Le Bouar, A. Loiseau, H. Pascard, *ibid.*, p. 761.
19. N. G. Chopra *et al.*, *Science* **269**, 966 (1995); O. Stephan *et al.*, *ibid.* **266**, 1683 (1994).
20. Mechanical properties of nanotubes and nanorods, such as elastic modulus and fracture strength, can be probed by using the lateral force sensing capabilities of the microscope to measure force versus displacement curves (E. W. Wong, P. E. Sheehan, C. M. Lieber, unpublished results).

21. We thank J. Liu and J. Huang for help in the design and fabrication of the electronics used in these measurements. C.M.L. acknowledges partial support of this work by the Materials Research Science and Engineering Center of the National Science Foundation under award DMR-9400396 and by the Office of Naval Research.

20 December 1995; accepted 22 February 1996

Teleconnections Between the Subtropical Monsoons and High-Latitude Climates During the Last Deglaciation

F. Sirocko,* D. Garbe-Schönberg, A. McIntyre, B. Molfino

The major deglacial intensification of the southwest monsoon occurred at 11,450 ± 150 calendar years before present, synchronous with a major climate transition as recorded in Greenland ice. An earlier event of monsoon intensification at 16,000 ± 150 calendar years before present occurred at the end of Heinrich layer 1 in the Atlantic and parallels the initial rise in global atmospheric methane concentrations and the first abrupt climate changes in the Antarctic; thus, the evolution of the monsoonal and high-latitude climates show teleconnections but hemispheric asymmetries. Superimposed on abrupt events, the monsoonal climate shows high-frequency variability of 1785-, 1450-, and 1150-year oscillations, and abrupt climate change seems to occur when at least two of these oscillations are in phase.

Major regions of the Northern Hemisphere are influenced either by Atlantic-controlled winds and precipitation or by the monsoons (Fig. 1). To evaluate physical links between these two large-scale systems, we compared their climatic history during the transition from the last glacial epoch into the Holocene as recorded in Greenland ice cores and in deep-sea sediments from the Arabian Sea. First observed by Dansgaard *et al.* (*1*) and confirmed by the ice cores of the Greenland Ice Core Project (GRIP) and Greenland Ice Sheet Project II (GISP2) (*2, 3*), the first abrupt deglacial warming event over the North Atlantic and Greenland occurred 14,500 ± 150 calendar years before present (B.P.), followed by another warming event at 11,600 ± 150 calendar years B.P. (Fig. 2). The increase in global atmospheric methane concentrations, in contrast, as recorded in the GRIP ice core, started about 16,000 calendar years B.P. (*4*), indicating an early onset of environmental change in the tropics, where most of the modern methane is produced in wetlands. The first deglacial change in wind trajectories and dust content over Antarctica also started at about 16,000 calendar years B.P. (*5*), that is, also significantly earlier than the first temperature increase in Greenland (Fig. 2). Accordingly, the climate of the high latitudes in the Northern and Southern hemispheres show strong regional contrasts.

To compare this asymmetric evolution of the polar climates with the evolution of the subtropical monsoons, we used data (*6*) from core 74KL from the upwelling area of the western Arabian Sea (Fig. 1), where five abrupt $\delta^{18}O$ changes have been ob-

F. Sirocko and D. Garbe-Schönberg, Geological-Paleontological Institute, University Kiel, Olshausenstrasse 40-60, 24118 Kiel, Germany.
A. McIntyre and B. Molfino, Lamont-Doherty Earth Observatory, Palisades, NY 10964, USA.

*To whom correspondence should be addressed at Geoforschungszentrum Potsdam, Am Telegrafenberg A17, 14473 Potsdam, Germany.